Chaos, Solitons and Fractals 146 (2021) 110812

Contents lists available at ScienceDirect

Chaos, Solitons and Fractals

Nonlinear Science, and Nonequilibrium and Complex Phenomena

journal homepage: www.elsevier.com/locate/chaos

Synchronization of interacted spiking neuronal networks with inhibitory coupling

Andrey V. Andreev[a,*], Vladimir A. Maksimenko[a,b], Alexander N. Pisarchik[c,a], Alexander E. Hramov[a,b]

[a] Neuroscience and Cognitive Technology Laboratory, Center for Technologies in Robotics and Mechatronics Components, Innopolis University, Universitetskaya, 1, Innopolis, 420500, Russia
[b] Saratov State Medical University, Bolshaya Kazachia st., 112, Saratov, 410012, Russia
[c] Center for Biomedical Technology, Universidad Politécnica de Madrid, Campus Montegancedo, 28223 Pozuelo de Alarcon, Spain

ARTICLE INFO

Article history:
Received 18 September 2020
Accepted 21 February 2021

Keywords:
Spiking neural network
Hodgkin-Huxley model
Synchronization

ABSTRACT

The development of mathematical models to describe neuronal interaction processes in the brain is a challenging task of nonlinear dynamics. Recent advances in biochemistry and neuroscience allow better understanding of biological mechanisms underlying the neuron functioning and synaptic connections between neurons. Moreover, significant progress in brain imaging sheds light on the structure of the brain network and certain aspects of neuronal dynamics. However, dynamical mechanisms leading to synchronization between different brain areas still remain unknown and require further investigation. To shed light on this issue, we consider two small-world networks of Hodgkin-Huxley neurons interacting via inhibitory coupling. We found that synchronization indices (SI) in both networks oscillate periodically in time, so that time intervals of high SI alternate with time intervals of low SI. Depending on the coupling strength, the two coupled networks can be in the regime of either in-phase or anti-phase synchronization. We suppose that the inherent mechanism behind such a behavior lies in the cognitive resource redistribution between neuronal ensembles of the brain.

1. Introduction

The application of the complex network theory to neuroscience is very promising for analyzing structural and functional connectivity of brain neurons [1]. Different mathematical models were used to describe the dynamics of a single neuron as a node of the neuronal network and the interaction between the neurons. Among them one can highlight the integrate-and-fire [2], Morris-Lecar [3], FitzHugh-Nagumo [4,5], Hindmarsh-Rose [6], and Hodgkin-Huxley (HH) [7] models. The HH model is the most complete bio-inspired model that describes the initiation and propagation of the action potential taking into account ionic currents in the neuron's membrane. The spiking activity generated by this model simulates the electrical activity of a real neuron [8].

Collective neuronal activity plays an important role in brain functioning. According to the functional magnetic resonance imaging (fMRI) studies, the whole-brain network activity is generated through the interaction of multiple functional subnetworks during either a resting state or task accomplishing. The functional subnetworks include a dorsal attention network, a frontoparietal network, an executive control network, a default mode network, and other neuronal networks [9]. Although functional networks have different anatomical locations, they interact with each other and overlap during task accomplishing [10].

Collective processes resulted from the functional interaction between remote populations of cortical neurons subserve the cognitive performance during demanding tasks. For instance, when the task complexity is high brain engages additional resources by involving multiple neuronal populations. In the visual processing tasks, a small amount of the sensory information can be processed by the occipito-parietal network, while increasing information complexity requires additional activation of prefrontal regions [11–13]. Finally, collective neuronal activity underlies cognitive performance during prolonged cognitive tasks. In this case, the brain dynamically redistributes the cognitive load among multiple cortical regions [14].

Current understanding of neuronal communication highlights a vital role of phase coherence in functional interaction between remote neuronal ensembles. To illustrate this issue, let us consider

* Corresponding author.
E-mail address: a.andreev@innopolis.ru (A.V. Andreev).

https://doi.org/10.1016/j.chaos.2021.110812
0960-0779/

the interaction between a pair of neurons. When a presynaptic neuron fires, a neurotransmitter (protein) enters a synaptic cleft from the axon terminal and moves across the synapse to be bind with receptors in the postsynaptic neuron. The binding of the neurotransmitter may results in either excitation or inhibition of the postsynaptic neuron. In the brain, a postsynaptic neuron may receive both excitatory and inhibitory inputs from thousands of neurons simultaneously. At the same time, the postsynaptic neuron is primarily excited by inputs from those neurons whose action potentials are coherent with the action potential of the postsynaptic neuron. In the absence of the coherence, the input signal comes to the postsynaptic neuron at a random phase of its excitability cycle and therefore has a low connectivity performance. Thus, efficient communication between brain neurons can only be achieved if the neurons are in the phase synchronization state.

In electroencephalographic (EEG) experiments, phase coherent behavior of neural ensembles results in the increasing amplitude of the electric potential registered by the electrode on sensor or source level. Previous experimental studies highlighted the existence of phase synchronization between high-frequency spiking activity of single neurons and low-frequency electric activity in the human brain. In particular, Canolty et al. [15] observed that the high-frequency γ-wave (80–150 Hz) of the electrocorticogram is modulated by the low-frequency θ-rhythm (4–8 Hz) envelope. Furthermore, different behavioral tasks evoked distinct patterns associated with of the θ – high-frequency γ coupling across the cortex. Their results evidenced that the coupling between low- and high-frequency brain rhythms coordinates the activity in distributed cortical areas, providing a mechanism for effective communication during cognitive processing in humans.

The high amplitude of electric potentials in the occipital and temporal cortical regions may indicate increasing coherence between neurons within local ensembles during earlier visual or auditory processing stages. To integrate sensory information from multiple sources or to perform more complex cognitive processing, the brain coordinates the activity of the distant ensembles. The latter requires phase coupling between low- and high-frequency brain rhythms. Thus, phase coherence is needed for forceful interaction between neural ensambles.

Although the neuroimaging studies provide substantial evidence for the vital role of phase coherence, dynamical mechanisms underlying the coherence within and between neuronal ensembles remain unclear. To address this issue, we simulate two inhibitory coupled networks of Hodgkin-Huxley neurons which receive the input signal in the form of a spike train. We observe that the synchronization index (SI) between the neurons in both networks periodically changes in time: time intervals of high SI alternate with time intervals of low SI. Adjusting the inhibitory coupling strength between the neural ensembles can result in either in-phase or anti-phase SI oscillations in the ensembles. We assume that in-phase mode is associated with coordination of the ensembles to perform a joint simultaneous cognitive operation, whereas anti-phase mode subserves their involvement in the task switching between two neuronal ensembles. Finally, we hypothesize that inhibitory coupling contributes to the controlling phase coherence between two neuronal populations.

2. Mathematical model

In this paper, we use the Hodgkin-Huxley (HH) model to describe the time evolution of the transmembrane potential of each neuron [7]:

$$C_m\frac{dV_i}{dt} = -g_{Na}^{max}m_i^3h_i(V_i-V_{Na}) - g_K^{max}n_i^4(V_i-V_K) - g_L^{max}(V_i-V_L) + I_i^{ex} + I_i^{syn} \quad (1)$$

where $C_m = 1\ \mu\text{F/cm}^3$ is the capacity of cell membrane, I_i^{ex} is the external bias current injected into a neuron in the network, V_i is the membrane potential of i-th neuron, $i = 1,\dots,N$ (N being the total number of neurons in the network) is the neuron number, $g_{Na}^{\max} = 120\ \text{mS/cm}^2$, $g_K^{\max} = 36\ \text{mS/cm}^2$, and $g_L^{\max} = 0.3\ \text{mS/cm}^2$ receptively denote the maximal sodium, potassium and leakage conductance when all ion channels are open. $V_{Na} = 50$ mV, $V_K = -77$ mV, $V_L = -54.4$ mV are the reversal potentials for sodium, potassium and leak channels, respectively, and I_i^{syn} is the total synaptic current received by neuron i. m, n and h represent the mean ratios of open gates of the specific ion channels. n^4 and m^3h are the mean portions of the open potassium and sodium ion channels within a membrane patch. The dynamics of the gating variables ($x = m, n, h$) is described as follows

$$\frac{dx_i}{dt} = \alpha_{x_i}(V_i)(1-x_i) - \beta_{x_i}(V_i)x_i + \xi_{x_i},\ (x = m, n, h), \quad (2)$$

where $\alpha_x(V)$ and $\beta_x(V)$ are rate functions defined as

$$\alpha_{m_i}(V_j) = \frac{0.1(25-V_i)}{e^{(25-V_i)/10}-1},\ \alpha_{n_i}(V_i) = \frac{0.01(10-V_i)}{e^{(10-V_i)/10}-1},$$
$$\alpha_{h_i}(V_i) = 0.07e^{-V_i/20},\ \beta_{m_i}(V_i) = 4e^{-V_i/18}, \quad (3)$$
$$\beta_{h_i}(V_i) = \frac{1}{1+e^{(30-V_i)/10}},\ \beta_{n_i}(V_i) = 0.125e^{-V_i/80},$$

In Eq. (2), ξ_{x_i} is independent zero mean Gaussian white noise, whose autocorrelation functions are

$$\langle\xi_{m_i}(t)\xi_{m_i}(t')\rangle = \frac{2\alpha_{m_i}\beta_{m_i}}{N_{Na}(\alpha_{m_i}+\beta_{m_i})}\delta(t-t'), \quad (4)$$

$$\langle\xi_{h_i}(t)\xi_{h_i}(t')\rangle = \frac{2\alpha_{h_i}\beta_{h_i}}{N_{Na}(\alpha_{h_i}+\beta_{h_i})}\delta(t-t'), \quad (5)$$

$$\langle\xi_{n_i}(t)\xi_{n_i}(t')\rangle = \frac{2\alpha_{n_i}\beta_{n_i}}{N_K(\alpha_{n_i}+\beta_{n_i})}\delta(t-t'). \quad (6)$$

Here, $N_{Na} = \rho_{Na}S$ and $N_K = \rho_K S$ represent the total number of sodium and potassium channels within membrane patch ($\rho_{Na} = 60$ m^{-2} and $\rho_K = 18$ m^{-2} being sodium and potassium channel densities, respectively) and $S = 1$ is the membrane patch area of each neuron.

In this work, we consider the coupling via chemical synapses only. The synaptic current takes the form [16]

$$I_i^{syn} = \sum_{j\in\mathbb{Z}(i)}^{N} g_c\alpha(t-t_s^j)(E_{rev}-V_j), \quad (7)$$

where $\alpha(t)$ describes the temporal evolution of the synaptic conductance, g_c is the maximal conductance of the synaptic channel, t_s^j is the moment of time at which presynaptic neuron j fires, $E_{rev} = 50$ mV is the synaptic reversal potential, and $\mathbb{Z}(i)$ is the set of presynaptic neurons coupled with the i-th postsynaptic neuron, defined by the adjacency matrix. We suppose that $\alpha(t) = e^{-t/\tau_{syn}}\Theta(t)$, where $\Theta(t)$ is the Heaviside step function and $\tau_{syn} = 3$ ms.

Synchronization inside each network is quantified with the synchronization index defined as [17,18]:

$$\Xi = \sqrt{\frac{1}{T-t_0}\int_{t_0}^{T}\eta(t)dt}, \quad (8)$$

where t_0 and T are durations of transients and total time series, and $\eta(t)$ is the standard deviation given as

$$\eta(t) = \frac{1}{N}\sum_{i=1}^{N}\left(x^{(i)}(t)\right)^2 - \left(\frac{1}{N}\sum_{i=1}^{N}x^{(i)}(t)\right)^2. \quad (9)$$

The lower the synchronization index Ξ, the better the synchronization, so that $\Xi = 0$ means complete synchronization.

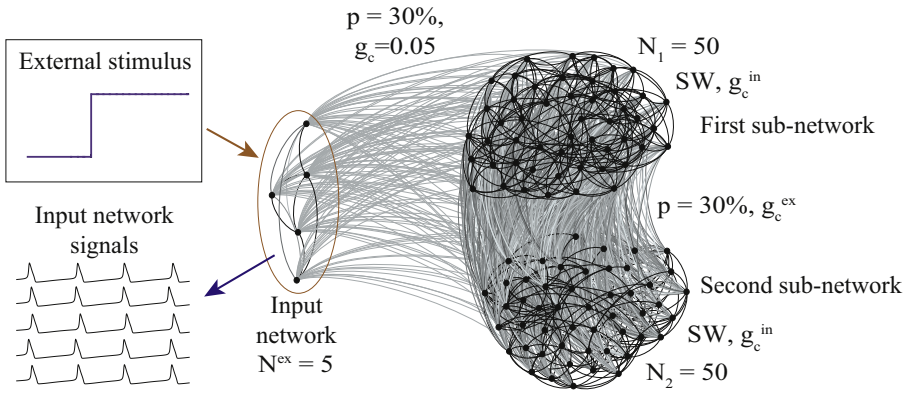

Fig. 1. Schematic of the network model. The external stimulus with amplitude A is applied to a small input network of $N^{ex} = 5$ neurons. Every neuron of the input network is unidirectionally connected to each of $N_1 = N_2 = 50$ neurons of two sub-networks by excitatory synapses with coupling strength $g_c = 0.05$ and probability $p = 30\%$. The sub-networks are bidirectionally connected to each other by inhibitory synapses with coupling strength g_c^{ex} and probability $p = 30\%$. The neurons Inside the sub-networks are connected to each other according to "small-world" (SW) topology with coupling strength g_c^{in}.

The correlation between interacted N_1 and N_2 sub-networks can be found on the base of their synchronization indices Ξ_1 and Ξ_2. The Pearson's linear correlation coefficient is calculated as follows [19]

$$r = \frac{\int_{t_0}^{T}(\Xi_1(t) - \overline{\Xi}_1)(\Xi_2(t) - \overline{\Xi}_2)dt}{\sqrt{\int_{t_0}^{T}(\Xi_1(t) - \overline{\Xi}_1)^2(\Xi_2(t) - \overline{\Xi}_2)^2 dt}}. \quad (10)$$

Here, $r = 1$ and $r = -1$ mean perfect positive and perfect negataive correlation, respectively.

3. Results and discussion

We consider the network presented in Fig. 1. The external stimulus of a constant current with amplitude A is applied to a small input network of $N^{ex} = 5$ neurons coupled with a randomly chosen coupling strength in the range $g_c^s \in [0, 0.15]$. This small network is unidirectionally connected to two large networks of $N_1 = N_2 = 50$ neurons by excitatory synapses with coupling strength $g_c = 0.05$ and probability $p = 30\%$. The large networks are bidirectionally connected to each other by inhibitory synapses with coupling strength g_c^{ex} and probability $p = 30\%$. The large networks have a "small-world" (SW) topology, and the neurons inside these networks are coupled with coupling strength g_c^{in}. We consider the SW network topology because we wish to simulate signal processing in the brain on both low-level and high-level stages, i.e, on the levels of a single neuron and neural ensembles. A continuous stimulus received by the small input network (N^{ex}) is transformed by the network into a sequence of neural spikes transmitted then to the large networks to process the signal.

The dynamical behavior of the sub-networks N_1 and N_2 is illustrated in Fig. 2(a). The first 50 neurons in the graph belong to the N_1 sub-network, while the second 50 neurons to the N_2 sub-network. The neurons inside each sub-network are coupled by inhibitory synapses, while the two sub-networks are interconnected via excitatory synapses. The type of synchronization beween the sub-networks depends on the coupling strength g_c^{ex}.

The dependence of the average spike amplitude $x_{avr} = \frac{1}{N_1}\sum_{i=1}^{N_1} x_i$ of the sub-network N_1 versus Ξ_1 is presented in Fig. 2(b). One can see that larger spike amplitude of the averaged signal corresponds to higher Ξ_1 with the correlation between them to be $r = 0.707$.

Using Eq. (8), we calculate the time series $\Xi_1(t)$ and $\Xi_2(t)$ and then filter them with a $[0.004, 0.015]$-Hz band-pass filter to visualize a slow variation of the macroscopic signal generated by each network. The result is presented in Fig. 2(c), where one can see that SIs of the two sub-networks oscillate periodically in time exhibiting antiphase synchronization [20].

Fig. 2 illustrate network dynamics for the coupling strengths $g_c^{ex} = -0.1$ and $g_c^{in} = 1.0$ between the large networks and inside them, respectively. One can see that in this case Ξ_1 and Ξ_2 are negatively correlated, i.e, their amplitudes oscillate approximately in antiphase. When Ξ_1 increases, Ξ_2 decreases and vice versa. We find that the type of synchronization depends on both g_c^{ex} and g_c^{in}.

The neurons inside each network fire at different moments of time. For time moments corresponding to the maximum values of the oscillating SI in each sub-network (shown by the arrows in Fig. 2(c)), we calculate the distributions of the time lags for all neurons in both sub-networks with respect to the average spike time. The resulting distributions for three SI maxima are present in Fig. 2(d). For both interacted networks N_1 and N_2 the distributions at t_1 and t_3 are similar to each other, while the distribution at t_2 is different. This is because t_1 and t_3 are times corresponding to the maximal Ξ_1, i.e, in the first network, while t_2 to the maximal Ξ_2, i.e., in the second network. The former distributions have pronounced peaks close to 0, while the latter distributions are wide and close to uniform.

In Fig. 3(a) we plot the two-parametric diagram of the correlation r of SIs in the space of g_c^{ex} and g_c^{in}. One can note the light yellow area of high positive correlation with a 0.02 width in the coupling strength g_c^{ex} between the sub-networks. The boundary values of this area increases as the coupling strength inside the networks (g_c^{in}) is decreased. Hence, to achieve maximal positive correlation, both coupling strengths must oscillate inphase, either decrease or increase simultaneously. This suggests that the excitatory current received by a neuron from the neurons of the same network and the inhibitory current received from another network should compensate each other. In a similar way, a maximal anticorrelation can be achieved (black areas in Fig. 3(a)) when two sub-networks demonstrate antiphase dynamics. One can also note that the upper dark area of negative correlation in Fig. 3(a) ($-0.06 < g_c^{ex} < -0.015$) is the widest for $g_c^{in} = 1.0$ and becomes narrower with decreasing the last one.

In Fig. 3(b) we plot the dependencies of the correlation r on the coupling strength between the large networks for different values of the coupling strength inside these networks. When the networks are disconnected ($g_c^{ex} = 0$), the correlation is close to $r = 0.15$. A decrease in the coupling strength g_c^{ex} towards more negative values first leads to a small increase in the correlation up to $r \in [0.2, 0.4]$. Then, a further decrease in g_c^{ex} results in a decrease in r to negative values up to $r \approx -0.8$ for $g_c^{ex} \approx -0.3$. After that, r grows again and reaches $r \approx 0.9$ for $g_c^{ex} \in [-0.055, -0.07]$ depending on g_c^{in}. For a

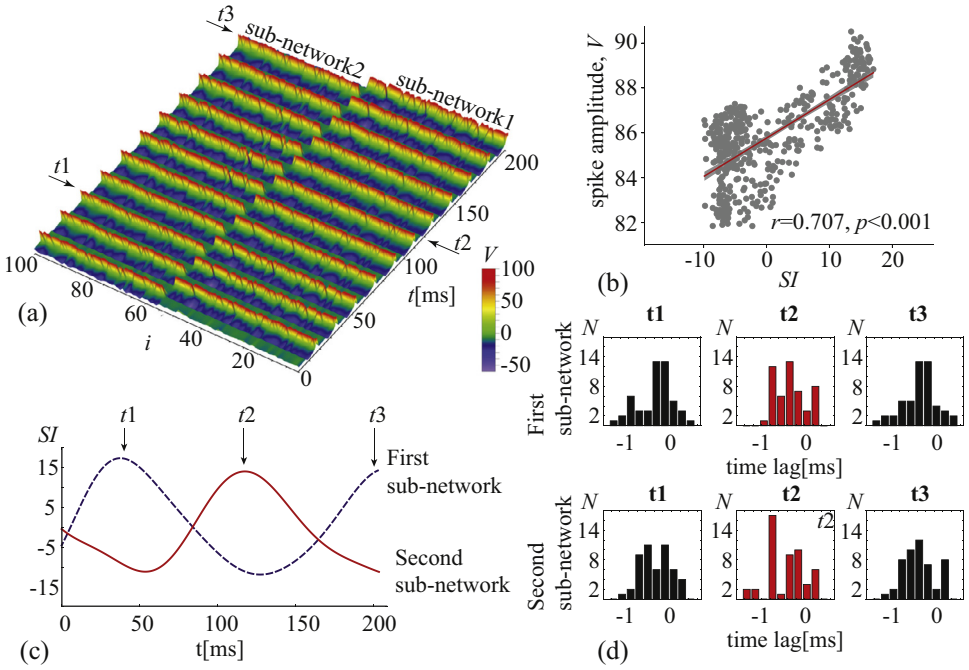

Fig. 2. (a) Time-space diagram of membrane potential V of neurons in the first N_1 ($1 \le i \le 50$) and second N_2 ($51 \le i \le 100$) sub-networks. (b) Spike amplitude of the signal averaged over all neurons of sub-network N_1 versus synchronization index (SI). The red line is the linear approximation with correlation $r = 0.707$ ($p < .001$). (c) Time evolution of SIs for two sub-networks, exhibiting antiphase dynamics. The arrows show the local maxima. (d) Distributions of spike lags of all neurons in the first (upper row) and second (lower row) sub-networks with respect to the average spike time. $g_c^{ex} = -0.1$, $g_c^{in} = 1.0$. (For interpretation of the references to colour in this figure legend, the reader is referred to the web version of this article.)

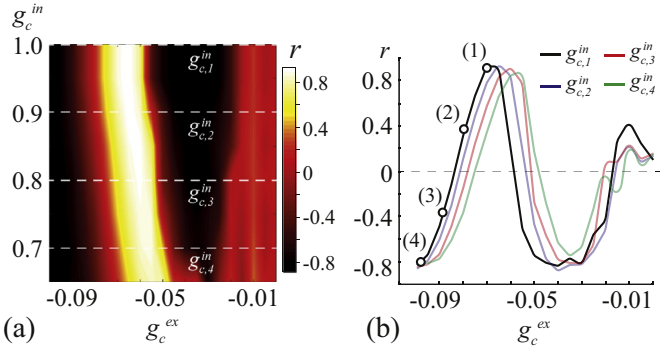

Fig. 3. (a) Two-parametric diagram of correlation r between synchronization indices of two sub-networks in the space of the coupling strengths between (g_c^{ex}) and inside (g_c^{in}) the networks. The points (1), (2), (3), and (4) correspond to the coupling strengths $g_c^{in} = 1.0$, 0.9, 0.8, and 0.7, respectively.

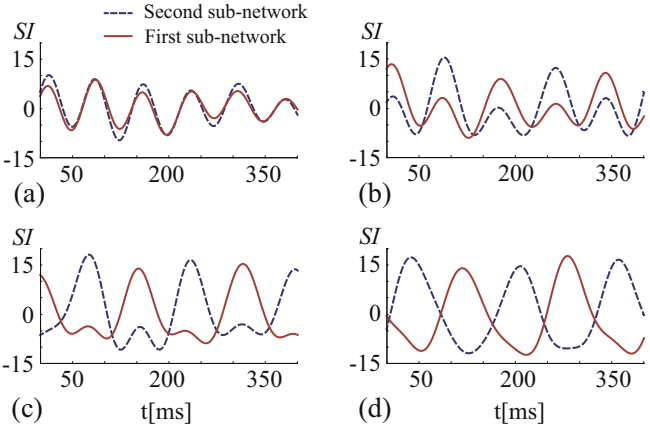

Fig. 4. Time series of synchronization indices (Ξ_1 and Ξ_2) for $g_c^{in} = 1.0$ and (a) $g_c^{ex} = -0.07$, (b) -0.08, (c) -0.09, and (d) -0.1. The correlation values corresponding to (a)-(c) are marked in Fig. 3(b) by (1)-(4).

smaller coupling strength inside the large networks, the maximum and minimum values of the correlation are achieved for a smaller coupling strength between the networks.

The time series of SIs are shown in Fig. 4 for three different values of the coupling strength between the large networks g_c^{ex}. While SI oscillates inphase for g_c^{ex} close to 0 (Fig. 4(a)), for higher negative values of g_c^{ex} these oscillations are asynchronous (Fig. 4(b,c)), and for $g_c^{ex} = 0.1$ they oscillate in antiphase (Fig. 4(d)).

The collective processes resulted from the functional interaction between remote populations of cortical neurons were shown to subserve the cognitive performance during demanding tasks. For instance, when the task complexity is high, the brain engages additional resources by involving multiple neuronal populations. The collective neuronal activity underlies the cognitive performance during prolonged cognitive tasks. In this case, the brain dynamically redistributes the cognitive load among multiple cortical regions. Here, we demonstrate that SI in both networks periodically oscillates in time; the time intervals with high SI alternate with the time intervals where SI is low. When adjusting the strength of inhibitory coupling, one can observe that SIs of these networks are inphase or antiphase synchronization. We can suppose that the underlying mechanism of antiphase oscillations stands behind the cognitive resource redistribution between neuronal ensembles in the brain.

All previous studies were performed for the case when the neurons of the small input network were connected to each other with a coupling strength randomly chosen from $g_c^s = 0$ to range $g_c^s = 0.15$. To investigate how the input signal from the small input network N^{ex} affects antiphase oscillations of the large networks, we fix the coupling strength g_c^s. In Fig. 5(a) we show how the cor-

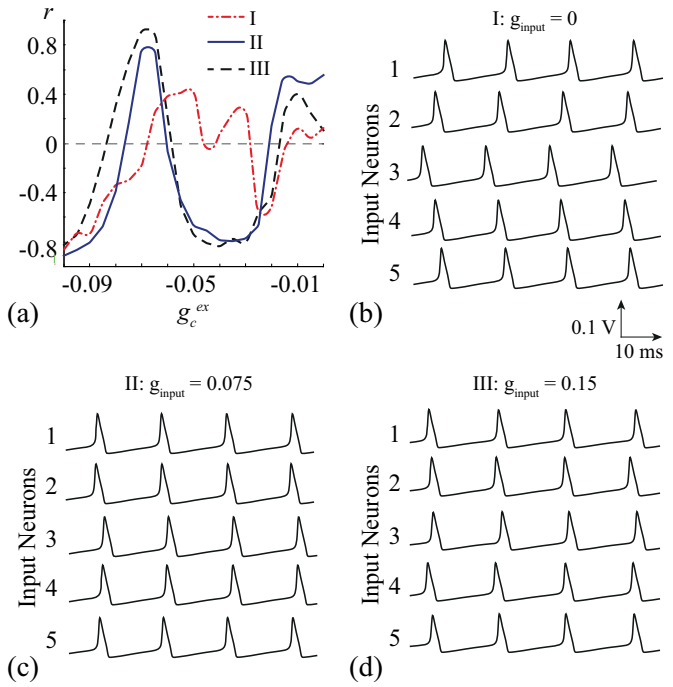

Fig. 5. (a) Correlation between synchronization indices r versus coupling strength g_c^{ex} between the sub-networks for different coupling strengths inside the small input network: I: $g_c^s = 0.15$, II: $g_c^s = 0.075$, III: $g_c^s = 0$. (b-d) Membrane potentials of input neurons for I, II and III.

relation changes for three different fixed values of g_c^s: $g_c^s = 0.15$ (red dash-dotted line I), $g_c^s = 0.075$ (solid blue line II), and $g_c^s = 0$ (black dashed line III). One can see that the dependences II and III are very similar. However, the elimination of the coupling in the input network (line I) leads to a decrease in the amplitude of correlation oscillations. The shape of line III differs from others. In Figs. 5(b-d), one can see that without coupling the neurons display asynchronous dynamics, while an increase in g_c^s improves synchronization between the neurons.

Thus, the increasing coupling between the neurons in the small input network N^{ex} affects synchronization in the large networks. Considering that the input network plays a role of low-level signal processing, the communication between neurons in this network is necessary for effective signal processing. It should be noted that regardless of the coupling strength in the input network, there is always decreasing SI correlation from positive ($r = 0.4$ or higer) to negative ($r = -0.8$) values for $g_c^{ex} < -0.06$. Therefore, we can assume that this process is determined by the interaction between N_1 and N_2 networks via inhibitory coupling.

4. Conclusion

In this paper we have investigated dynamics of the complex network of Hodgkin-Huxley neurons. The considered network consisted of a small input network and two large interacted networks. An external signal received by the input network was transformed by the network into a sequence of spikes, and then transmitted to two sub-networks of small-world configuration, interacting with each other via an inhibitory coupling and operating together to process the signal.

We have observed that the synchronization index (SI) in both networks oscillates periodically in time; the time intervals of high SI alternates with the time intervals of low SI. We have found that SIs in these networks exhibit either inphase or antiphase synchronization depending on the inhibitory coupling strength between them. We suppose that the underlying mechanism behind the antiphase dynamics lies in the cognitive resource redistribution between neuronal ensembles in the brain.

We have also demonstrated that excitatory coupling between the neurons inside the network affects the synchronization index. To maintain the neural network in the regimes of inphase or antiphase SI oscillations, we should keep a balance between excitatory and inhibitory connections. It suggests that the excitatory and the inhibitory currents should compensate each other. In other words, when one of them increases, the other must be increased too, and vice versa.

Finally, we have shown that the coupling inside the input small network affects antiphase synchronization between two large networks. However, the scenario from positive and negative correlation and back between the large networks are only determined by inhibitory coupling between them.

Declaration of Competing Interest

The authors declare that they have no known competing financial interests or personal relationships that could have appeared to influence the work reported in this paper.

Acknowledgments

V.A.M. received support from Russian Science Foundation (Grant 20-72-00036) in formulating the concept of mathematical model. A.V.A. was supported by Russian Foundation for Basic Research (Grant 18-32-20129) in numerical simulations. A.E.H. and A.N.P. acknowledge President Program for Leading Scientific School Supporting (Grant NSH-2594.2020.2) in the part of numerical results interpretation.

References

[1] Bullmore E, Sporns O. Complex brain networks: graph theoretical analysis of structural and functional systems. Nat Rev Neurosci 2009;10:186–98.
[2] Lapicque L. Recherches quantitatives sur l'excitation electrique des nerfs traitee comme une polarization. Journal de Physiologie et de Pathologie Generalej 1907;9:620–35.
[3] Morris C, Lecar H. Voltage oscillations in the barnacle giant muscle fiber. Biophys J 1981;35(1):193–213.
[4] FitzHugh R. Impulses and physiological states in theoretical models of nerve membrane. Biophys J 1961;1(6):445.
[5] Nagumo J, Arimoto S, Yoshizawa S. An active pulse transmission line simulating nerve axon. Proc IRE 1962;50(10):2061–70.
[6] Hindmarsh JL, Rose R. A model of neuronal bursting using three coupled first order differential equations. Proc Royal Soc London Series B Biological Sciences 1984;221(1222):87–102.
[7] Hodgkin A, Huxley A. A quantitative description of membrane current and its application to conduction and excitation in nerve. J Physiol 1952(117):500–44.
[8] Wang Q, Perc M, Duan Z, Chen G. Delay-enhanced coherence of spiral waves in noisy hodgkin–huxley neuronal networks. Phys Lett A 2008;372(35):5681–7.
[9] Van MP, Van MP, Den H. Exploring the brain network: a review on resting-state fmri functional connectivity. Eur Neuropsychopharmacol 2010;20(8):519–34.
[10] Xu J, Potenza MN, Calhoun VD. Spatial ica reveals functional activity hidden from traditional fmri glm-based analyses. Front Neurosci 2013;7:154.
[11] Pisarchik AN, Maksimenko VA, Andreev AV, Frolov NS, Makarov VV, Zhuravlev MO, Runnova AE, Hramov AE. Coherent resonance in the distributed cortical network during sensory information processing. Sci Rep 2019;9(1):1–9.
[12] Maksimenko VA, Frolov NS, Hramov AE, Runnova AE, Grubov VV, Kurths J, Pisarchik AN. Neural interactions in a spatially-distributed cortical network during perceptual decision-making. Front Behav Neurosci 2019;13:220.
[13] Frolov NS, Maksimenko VA, Khramova MV, Pisarchik AN, Hramov AE. Dynamics of functional connectivity in multilayer cortical brain network during sensory information processing. Eur Phys J Spec Top 2019;228(11):2381–9.
[14] Uhlhaas P, Pipa G, Lima B, Melloni L, Neuenschwander S, Nikolić D, Singer W. Neural synchrony in cortical networks: history, concept and current status. Front Integr Neurosci 2009;3:17.
[15] Canolty RT, Edwards E, Dalal SS, Soltani M, Nagarajan SS, Berger MS, Barbaro NM, Knight RT, kirsch He. High gamma power is phase-locked to theta oscillations in human neocortex. Science 2006;313(5793):1626–8.
[16] White JA, Rubinstein JT, Kay AR. Channel noise in neurons. Trends Neurosci 2000;23(3):131–7.

[17] Wang Q, Perc M, Duan Z, Chen G. Synchronization transitions on scale-free neuronal networks due to finite information transmission delays. Phys Rev E 2009;80(2):026206.
[18] Pisarchik A, Sausedo-Solorio J. Synchronization in network motifs of delay-coupled map-based neurons. Eur Phys J Spec Top 2017;226(9):1911–20.
[19] Fisher RA. Statistical methods for research workers. in: Breakthroughs in Statistics, Springer 1992:66–70.
[20] Boccaletti S., Pisarchik A.N., del Genio C.I., Amann A.. Cambridge univ. press. 2018.